Resonance gaps and slow sound in three-dimensional phononic crystals: Rod-in-a-box paradigm

Kenny L. S. Yip [*] and Sajeev John [†]

Department of Physics, University of Toronto, 60 St. George Street, Toronto, Ontario, Canada M5S 1A7

We introduce a rod-in-a-box model for acoustic resonators. For resonators small compared to the acoustic wavelength, an elastostatic equilibrium approximation yields closed-form expressions for their frequency-dependent effective masses and moments of inertia. The low-frequency bands and gaps are recaptured by an intuitive 6×6 matrix eigenvalue equation, yielding a band structure within 2.3% agreement with the finite-element method. Our model is generalized to complex dumbbell-shaped resonators, revealing a dense collection of flat "slow sound" bands near the resonance band gap.

Phononic crystals are periodic composites of elastic materials, extensively studied for sound wave engineering [1–20]. Rapid and accurate fabrication of three-dimensional (3D) phononic crystals has been achieved through advances in additive manufacturing [21–26]. Conventional nonresonant phononic crystals require large feature sizes compared to acoustic wavelengths to provide sonic control. This is impractical at audible frequencies. Local resonators, which typically consist of dense cores surrounded by an elastically soft material and encapsulated by a hard shell, overcome this scaling problem and facilitate deep subwavelength manipulation of sound [27–30]. In this Letter, we introduce a simple physical model that accurately recaptures the low-frequency phononic modes of a medium with complex multiple coupled local resonances. This model offers physical insight into the coupling of resonators with internal translational and rotational degrees of freedom. Resulting applications of subwavelength "sound engineering" include noise mitigation in thin films, acoustic collimation, and sonic imaging.

The effective inertia-spring tensor (EIST) model [31] recaptures the salient mechanical responses of a locally resonant acoustic medium. The low-frequency response of coupled resonators is often dominated by a small number of macroscopic variables. Those responsible for the coupling between resonators are referred to as the shell variables $\{X_i\}$. The internal degrees of freedom, called core variables, can be represented by frequency-dependent terms in an effective inertia tensor m_{ij}. In a linear elastic medium, there is a general linear map from the shell displacements to the generalized forces, which we refer to as the spring tensor k_{ij}. It governs the interaction among spatially separated resonators in the phononic crystal. It depends on the lattice arrangements, the wave vector $\mathbf{K}$, and the shell geometry, but is insensitive to the interior of the resonators. Together, the mode spectrum of a periodic array of coupled resonators is described by a generalized form of

Newton's second law:

$$m_{ij}(\omega)\ddot{X}_j = -k_{ij}(\mathbf{K})X_j. \tag{1}$$

In elastic systems, force is a dynamic quantity described by an external stress tensor, whereas acceleration is a kinematic quantity specified by length and time measurements. The concept is extended to harmonically driven resonators. Without prior knowledge of the interior structure of a resonator, an observer tabulates such a ratio at each frequency, yielding a frequency-dependent effective inertia.

The predominant degrees of freedom of a rigid body are translations and rotations in orthogonal directions. In three dimensions, the low-frequency response of a resonator is dominated by six effective inertial quantities, which are its effective masses and principal moments of inertia in three orthogonal directions. The complete collection of effective inertial quantities constitutes the effective mass tensor $m_{ij}(\omega)$.

In general, the effective inertia tensor gains a pair of nonzero off-diagonal elements, when symmetry is broken, as depicted in Fig. 1(a). The resonator consists of a rigid box of mass m_{s} uniformly distributed along its left sidewall, and transverse moment of inertia I_{s} about its center of mass. All other walls are assumed to be massless. The box is coupled to a thin uniform interior rod of mass m_{c} and transverse center-of-mass moment of inertia I_{c}, through a pair of identical massless springs [32] of spring constant $\kappa/2$. The linear (angular) displacements of the shell and the core are denoted by x_{s} (ϕ_{s}) and x_{c} (ϕ_{c}), respectively. The connecting points of the springs are separated by a distance $2d$, individually located at $(a+d)$ and $(a-d)$ from the center of rotation of the box. The box is harmonically driven by an external force $f_{\mathrm{b}}e^{-i\omega t}$ and external torque $\tau_{\mathrm{b}}e^{-i\omega t}$. The extensions of the upper ϵ_{+} and lower ϵ_{-} springs, for small ϕ_{s} and ϕ_{c}, are expressed in terms of the mechanical variables of the box and the rod:

$$\epsilon_{\pm} = -x_{\mathrm{s}} + (a \pm d)\phi_{\mathrm{s}} + x_{\mathrm{c}} \mp d\phi_{\mathrm{c}}. \tag{2}$$

─────────
*Corresponding author: lskyip@physics.utoronto.ca
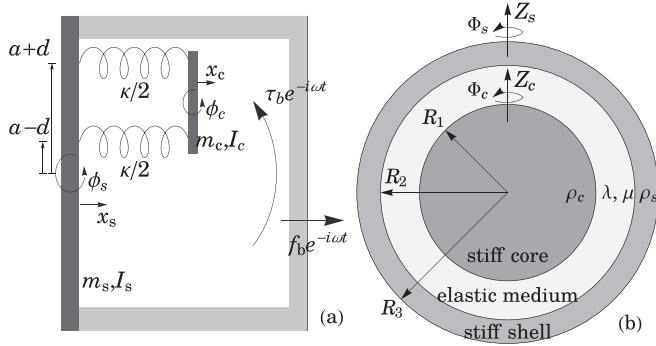†john@physics.utoronto.ca

L060306-1

FIG. 1. (a) A rigid box is coupled to an interior rod via a pair of massless springs. The masses of the rod and box are limited to and evenly distributed over the dark shaded regions. The shell and the core oscillate translationally and rotationally. The resonator is harmonically driven by an external force and an external torque about the box center of mass. (b) A 3D radially symmetric resonator consists of a dense and stiff core, embedded in an elastic material, encapsulated by a spherically annular stiff shell. The core and the shell are treated as rigid bodies. The interstitial elastic material is approximated as a massless elastic spring under elastostatic equilibrium.

All components oscillate at the driving angular frequency ω in the steady state:

$$m_s \ddot{x}_s = (\kappa/2)(\epsilon_+ + \epsilon_-) + f_b e^{-i\omega t}, \tag{3a}$$

$$I_s \ddot{\phi}_s = -(\kappa/2)[(a+d)\epsilon_+ + (a-d)\epsilon_-] + \tau_b e^{-i\omega t}, \tag{3b}$$

$$m_c \ddot{x}_c = -(\kappa/2)(\epsilon_+ + \epsilon_-), \tag{3c}$$

$$I_c \ddot{\phi}_c = (\kappa d/2)(\epsilon_+ - \epsilon_-). \tag{3d}$$

By Eqs. (3c) and (3d), the mechanical variables of the core can be expressed in terms of those of the shell. These are substituted into Eqs. (3a) and (3b) to yield a generalized form of Newton's second law,

$$\begin{pmatrix} m_{11}(\omega) & m_{12}(\omega) \\ m_{21}(\omega) & m_{22}(\omega) \end{pmatrix} \begin{pmatrix} \ddot{x}_s \\ \ddot{\phi}_s \end{pmatrix} = \begin{pmatrix} f_b e^{-i\omega t} \\ \tau_b e^{-i\omega t} \end{pmatrix}, \tag{4}$$

where the components of the symmetric effective inertia tensor $m_{ij}(\omega)$ are

$$m_{11}(\omega) = m_s (\omega_{*,t}^2 - \omega^2)/(\omega_{0,t}^2 - \omega^2), \tag{5a}$$

$$m_{12}(\omega) = m_{21}(\omega) = -m_c a \omega_{0,t}^2 /(\omega_{0,t}^2 - \omega^2), \tag{5b}$$

$$m_{22}(\omega) = I_s (\omega_{*,r}^2 - \omega^2)/(\omega_{0,r}^2 - \omega^2) - a m_{12}(\omega). \tag{5c}$$

The distance between the spring connecting points measures the torsional spring constant for rotational oscillation $\kappa_r = \kappa d^2$. $\omega_{*,t} \equiv (\kappa/m_c + \kappa/m_s)^{1/2}$ denotes the zero-mass frequency of translational resonance, typically associated with the normal mode of the resonator. $\omega_{0,t} \equiv (\kappa/m_c)^{1/2}$ denotes the resonant frequency of translational resonance, which is the normal mode frequency when the resonator shell is spatially fixed. The effective mass diverges at the resonant frequency, because a tiny displacement of the shell corresponds to substantial motion of the core. The characteristic frequencies for rotational resonance are defined similarly: $\omega_{*,r} \equiv (\kappa_r/I_c + \kappa_r/I_s)^{1/2}$ and $\omega_{0,r} \equiv (\kappa_r/I_c)^{1/2}$ [33].

For a lattice of resonators in a background composed of linear elastic materials, there is a general linear map between
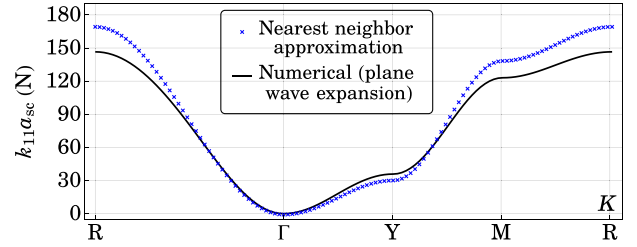

FIG. 2. Spring tensor component $k_{11}(\mathbf{K})$ is plotted for the nearest-neighbor approximation in Eq. (6) and numerical plane-wave expansion solution for $R/a_{sc} \approx 0.4924$, $b/a_{sc} \approx 0.3032$, $\lambda = 23.10$ kPa, and $\mu = 15.38$ kPa.

the generalized forces acting on the resonators and the generalized displacements of the resonator shell. This is referred to as the spring tensor k_{ij}. It describes the net forces and torques acting on a resonator, depending on the separation and relative motion of other resonators in the structure. For a periodic array of resonators, it is conveniently expressed in terms of Fourier components of the generalized displacement field, labeled by the wave vector $\mathbf{K}$.

The wave-vector dependence of the spring tensor can be roughly expressed by a nearest-neighbor approximation [34]. For illustration, we consider a lattice of spherical resonator shells of common radii R in a simple cubic lattice of lattice constant a_{sc}. Suppose the resonator centered at the origin displaces from the equilibrium by $X_s \hat{\mathbf{x}}$. By discrete translational symmetry, a resonator centered at $\mathbf{r}$ displaces at a phase difference $e^{i\mathbf{K}\cdot\mathbf{r}}$ relative to central resonator. The relevant elastic strain at $\mathbf{r}'$ on the surface of the central resonator can be estimated by their relative displacement $\mathrm{Re}[(e^{i\mathbf{K}\cdot\mathbf{r}} - 1)X_s]$, divided by the distance, $r - 2\mathbf{r}' \cdot \hat{\mathbf{r}}$, between the points on the surfaces of the adjacent spheres connected by a line parallel to $\mathbf{r}$. For longitudinal (transverse) disturbance in an isotropic elastic background defined by Lamé constants λ and μ, the strain is multiplied by $\lambda + 2\mu$ (2μ) to yield the stress. The elastic force acting on the central resonator, arising from the relative motion with the adjacent resonator, is estimated by an integral (over the primed variable) of the approximate stress on the surface of the central scatterer. Ignoring cross interactions, we add up the independent elastic forces due to relative motion with the six nearest neighbors at $\mathbf{r} = \pm a_{sc}\hat{\mathbf{x}}, \pm a_{sc}\hat{\mathbf{y}}, \pm a_{sc}\hat{\mathbf{z}}$ to obtain the nearest-neighbor approximation of the spring tensor component $k_{11}(\mathbf{K})$,

$$k_{11}(\mathbf{K}) \approx (4\pi R^2/b)\{(\lambda + 2\mu)[1 - \cos(K_x a_{sc})] + \mu[2 - \cos(K_y a_{sc}) - \cos(K_z a_{sc})]\}, \tag{6}$$

where $b = -2R[1 + (a_{sc}/2R)\log(1 - 2R/a_{sc})]^{-1}$ ranges from 0 to $2a_{sc}$ depending on the size and separation of the resonators. The wave-vector dependence of other spring tensor components can be estimated by symmetry arguments or similar analyses. The actual spring tensor is evaluated numerically by plane-wave expansion or a finite-element method, which includes forces from more distant resonators. For illustration, the spring tensor component $k_{11}(\mathbf{K})$ is plotted in Fig. 2, for a simple cubic lattice of rigid spherical resonators occupying 50% by volume in a background of open-cell foam. The nearest-neighbor approximation closely

resembles the wave-vector dependence of the full spring tensor.

For a 3D phononic crystal, the low-frequency response is described by a 6×6 Hermitian, positive-definite spring tensor. Intuitively, when a resonator shell at the origin rotates by $\Phi_s \hat{\mathbf{z}}$, the resonator at $\mathbf{r} = a\hat{\mathbf{x}}$ simultaneously experiences a force in the y direction and a torque in the z direction. The intricate coupling of the translational and rotational modes between spatially separated resonators is delineated in the spring tensor. Except at high-symmetry $\mathbf{K}$ points [31], the effective inertia tensor and spring tensor are not simultaneously diagonalizable. In the EIST model, between the resonant frequencies and zero-mass frequencies, the effective inertia tensor is negative definite, while the spring tensor is positive definite. Consequently, the eigenvalue problem (1) admits no real solution in ω. In other words, the simultaneous negativity of effective masses and moments of inertia signifies a resonance-based phononic band gap.

A typical resonator consists of a dense and stiff core, surrounded by a layer of light and elastically soft material, encapsulated by a stiff shell [27,28]. Over the acoustic frequency range of interest, the core and shell behave as rigid bodies with negligible shape deformation. The macroscopically defined linear and angular displacements of the core and shell are the predominant degrees of freedom. In contrast, the strain in the interstitial deformable material is not negligible. Nevertheless, we can approximate the light, soft medium as a massless spring that satisfies an elastostatic equilibrium. This is accurate when the relevant dimensions of a resonator are very small compared to the elastic wavelength. This rigid core-shell approximation (RCSA) was previously applied [31,35] to 2D cylindrically symmetric resonators to accurately recapture the out-of-plane translational, in-plane translational, and rotational resonances.

Here, we extend the RCSA analysis to a three-dimensional spherically symmetric resonator [Fig. 1(b)]. The dense spherical core of radius R_1 and mass density ρ_c is embedded in a spherically annular layer of isotropic, linear elastic foam of Lamé parameters λ and μ. The resonator is capped by a stiff shell of inner radius R_2, outer radius R_3, and density ρ_s. Radial symmetry requires that the translational or rotational motion of the core only couples to the same type of motion of the shell in the same direction. The 6×6 inertia tensor $m_{ij}(\omega)$ is diagonal, with $m_{11}(\omega)$, $m_{22}(\omega)$, and $m_{33}(\omega)$ being the effective masses, and $m_{44}(\omega)$, $m_{55}(\omega)$, and $m_{66}(\omega)$ being the effective moments of inertia.

When the core displaces from equilibrium by $Z_c \hat{\mathbf{z}}$ and the shell by $Z_s \hat{\mathbf{z}}$, the displacement field in spherical coordinates $\mathbf{u}(\mathbf{r}) = u_r(r) \cos\theta \hat{\mathbf{r}} + u_\theta(r) \sin\theta \hat{\boldsymbol{\theta}}$, with $R_1 < r < R_2$, satisfies elastostatic equilibrium under the boundary conditions $\mathbf{u}(R_{1/2}) = Z_{c/s}\hat{\mathbf{z}} = Z_{c/s}(\cos\theta \hat{\mathbf{r}} - \sin\theta \hat{\boldsymbol{\theta}})$. In the absence of an external body force, the stress tensor is divergence free and the displacement components $\{u_r, u_\theta\}$ satisfies a set of coupled second-order linear differential equations [36]. The boundary-value problem is solved in terms of elementary functions. The elastic force acting on the core/shell is calculated by surface integrals of the stress tensor on $\{r = R_{1/2}\}$. The translational equations of motion of the core and the shell can be mapped to a rod-in-a-box model ($a = 0$) in Eqs. (3a) and (3c), with the mass of the shell $m_s = (4\pi/3)\rho_s(R_2^3 - R_1^3)$, the mass of
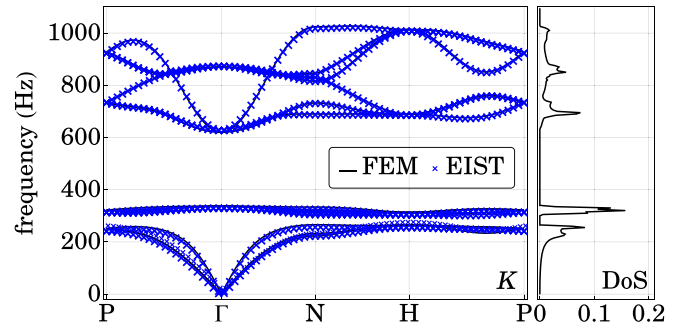

FIG. 3. The phononic band diagram of a bcc lattice of the spherical steel-cellulose resonators in foam background is evaluated, in the irreducible Brillouin zone, for the EIST model in Eq. (1) and FEM benchmark. The maximum percentage error is 2.32%. The normalized density of states confirms the complete acoustic band gap from 337 to 621 Hz.

the core $m_c = (4\pi/3)\rho_c R_1^3$, and the linear spring constant κ [37]. The result is readily applied to the widely cited, locally resonant sonic material [27], composed of centimeter-sized lead ball bearings, coated by a 2.5-mm layer of soft silicone. Our RCSA result predicts a resonant frequency $f_{0,\text{Liu}} \equiv \sqrt{\kappa/m_c}/(2\pi) \approx 380.9$ Hz [38], which matches the transmission dip and opening of phononic bad gap at 380 Hz (see Fig. 1 in Ref. [27]).

The rotational resonance is studied by a similar elastostatic equilibrium analysis [39]. The rotational equations of motion of the core and the shell can be mapped to a rod-in-a-box model ($a = 0$) in Eqs. (3b) and (3d): $I_s = (8\pi/15)\rho_s(R_2^5 - R_1^5)$, $I_c = (8\pi/15)\rho_c R_1^5$, and $\kappa_r = 8\pi\mu R_1^3 R_2^3/(R_2^3 - R_1^3)$.

We consider spherical resonators arranged in a body-centered-cubic (bcc) lattice of spacing $a_{\text{bcc}} = 2^{1/3}$ cm. The materials of the dense core, interstitial elastic medium, and stiff shell are, respectively, steel, open-cell foam, and cellulose, occupying 10%, 20%, and 20% by volume. Material constants are provided in Table 1 of Ref. [35]. By the results of RCSA, the characteristic frequencies are expressible in terms of rational functions of the lengths and elastic constants of the resonator. In this specific case, we calculate the resonant frequency $f_{0,\text{t}} \equiv \omega_{0,\text{t}}/(2\pi) \approx 320.0$ Hz and zero-mass frequency $f_{*,\text{t}} \equiv \omega_{*,\text{t}}/(2\pi) \approx 635.3$ Hz for translational resonance, as well as resonant frequency $f_{0,\text{r}} \equiv \omega_{0,\text{r}}/(2\pi) \approx 364.9$ Hz and zero-mass frequency $f_{*,\text{r}} \equiv \omega_{*,\text{r}}/(2\pi) \approx 476.0$ Hz for rotational resonance.

The mode spectrum is calculated in the EIST representation (1). The phononic band diagram and normalized density of states are plotted in Fig. 3. The eigenfrequencies agree with the finite-element method (FEM) numerical benchmark within 2.32% throughout the irreducible Brillouin zone. There is a complete phononic gap from 337 to 621 Hz, overlapping with the frequency interval where the effective masses and moments of inertia are simultaneously negative. The first six bands below the resonant frequencies are associated with the in-phase translational and rotational oscillations in three orthogonal directions of the steel ball and the cellulose shell. In contrast, the next six bands above the zero-mass frequencies correspond to the antiphase oscillations. The 13th band opens at 3700 Hz. The phononic gap of nearly 60% from the sixth
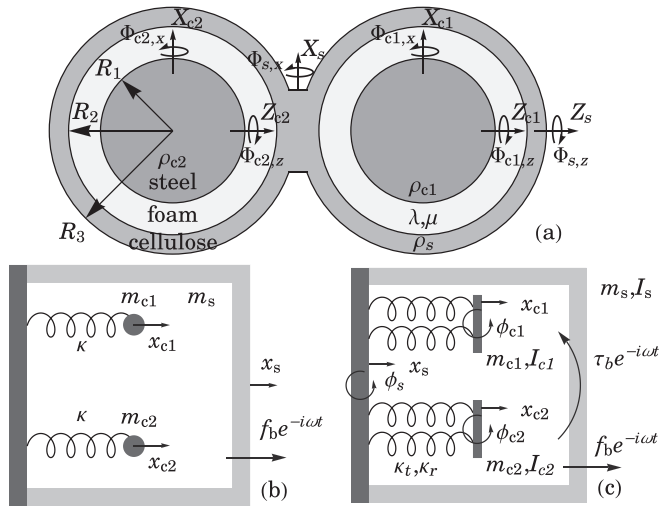
FIG. 4. The resonator consists of a dumbbell-shaped shell with two interior masses. The axial translational and rotational resonances are mapped to the two-masses-in-a-box model. Because of the off-center positions of the interior masses, lateral translation and rotation are intricately coupled. The internal couplings are represented by the two-rods-in-a-box model.
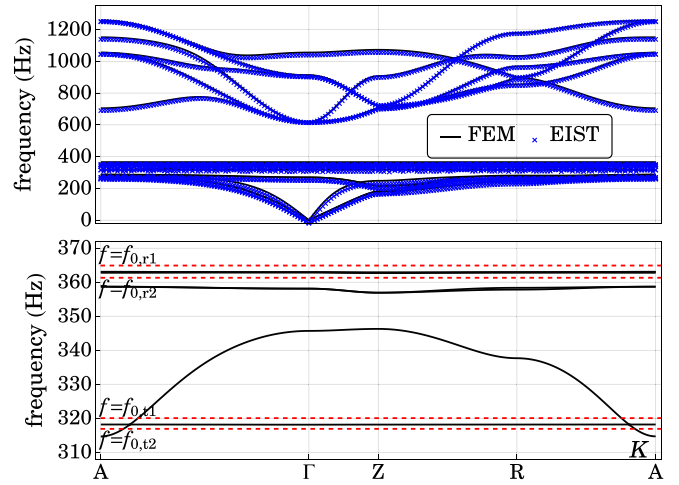

FIG. 5. The band diagram of a tetragonal lattice of the dumbbell resonators is plotted in the irreducible Brillouin zone, for the EIST model in Eq. (1) and FEM benchmark. The band diagram is zoomed in at the lower edge of the band gap, containing dense collections of phononic flat bands, sandwiched between the resonant frequencies.

to seventh band is caused by local resonances of individual resonators, and is likely very tolerant to small random displacements of the equilibrium positions of identical resonators. On the other hand, the gap between the 12th and 13th band arises from Bragg scattering of the periodic array and is likely to contain localized states of sound with positional disorder.

Our methodology is readily generalized to more complex resonator architectures. A dumbbell-shaped resonator has multiple coupled resonances, which reveal a dense collection of flat bands near its resonant frequencies. Such "slow sound" modes may be effective in trapping and absorbing sound in a thin film [40–42]. The compound resonator in Fig. 4(a) is formed by connecting two spherical core-shell resonators, separated by 1 cm, with a rigid handle of radius $(1/3)R_3$. One of the steel balls is assumed to be 2% denser to reflect natural variations in manufacturing. Axial translation and rotation, which are decoupled from the lateral motion by azimuthal symmetry, are mapped to a two-masses-in-a-box model of Fig. 4(b). In contrast, the lateral translation and rotation are intricately coupled, represented by off-diagonal effective inertia terms in a two-rods-in-a-box model of Fig. 4(c). In a generalization of Eqs. (5a)–(5c), the effective mass is

$$m_{33}(f) = m_{db} + \frac{m_{c1}f_{0,t1}^2}{f_{0,t1}^2 - f^2} + \frac{m_{c2}f_{0,t2}^2}{f_{0,t2}^2 - f^2}, \quad (7)$$

where $m_{c1} = (4\pi/3)\rho_{c1}R_1^3 \approx 7.940$ mg, $m_{c2} = 1.02m_{c1}$, $m_{db} \approx 0.5449$ mg [43]. With the same geometry of the interstitial foam, the same set of spring constants applies, and thus $f_{0,t1} = f_{0,t} \approx 320.0$ Hz and $f_{0,r1} = f_{0,r} \approx 364.9$ Hz. The second core is assumed to be 2% denser, so that the associated frequencies reduce by approximately 1%: $f_{0,t2} \approx 316.9$ Hz and $f_{0,r2} \approx 361.3$ Hz.

The dumbbell resonators are arranged with dumbbell axes oriented vertically in a tetragonal lattice with a square base of

1 cm and height 2 cm. A striking feature of the band diagram in Fig. 5 is the emergence of dense collections of phononic flat bands, between the translational resonant frequencies $f_{t1} < f < f_{t2}$ and the rotational resonant frequencies $f_{r1} < f < f_{r2}$. Since the group velocity of a wave packet is equal to the **K**-space gradient of the dispersion relation, these flat bands correspond to "slow sound modes" in three dimensions. Their occurrences can be inferred from the effective inertia tensor. For example, the axial effective mass $m_{33}(f)$ has three positive branches. At a given wave vector **K**, each positive branch yields an eigenfrequency by Eq. (1), which corresponds to a phononic band when evaluated throughout the irreducible Brillouin zone. The first branch $(f < f_{0,t2})$ is the in-phase translational oscillation of the shell and both cores. Over the third branch $(f_{0,t1} < f)$, the shell oscillates in antiphase relative to both cores. There is a narrow branch between the two resonant frequencies $(f_{0,t2} < f < f_{0,t1})$ that the shell is almost stationary while the two cores are in antiphase. Similar analyses apply to other translational and rotational modes. The canceling antiphase forces of the dense cores in the dumbbell resonator cause reactive flat bands between the two resonant frequencies.

In conclusion, we have shown the efficacy of a simple, intuitive, rod-in-a-box representation of complex local resonators in a 3D elastic medium. This reveals large resonance gaps, distinct Bragg gaps, and remarkable slow sound modes in the low-frequency acoustic spectrum. These may prove invaluable in noise mitigation and sculpting audible sound using thin coatings of absorbing, resonant elastic materials.

[1] M. S. Kushwaha, P. Halevi, L. Dobrzynski, and B. Djafari-Rouhani, Phys. Rev. Lett. **71**, 2022 (1993).

[2] M. S. Kushwaha, P. Halevi, G. Martínez, L. Dobrzynski, and B. Djafari-Rouhani, Phys. Rev. B **49**, 2313 (1994).

[3] F. R. Montero de Espinosa, E. Jiménez, and M. Torres, Phys. Rev. Lett. **80**, 1208 (1998).

[4] J. V. Sánchez-Pérez, D. Caballero, R. Mártinez-Sala, C. Rubio, J. Sánchez-Dehesa, F. Meseguer, J. Llinares, and F. Gálvez, Phys. Rev. Lett. **80**, 5325 (1998).

[5] J. O. Vasseur, P. A. Deymier, B. Chenni, B. Djafari-Rouhani, L. Dobrzynski, and D. Prevost, Phys. Rev. Lett. **86**, 3012 (2001).

[6] H. H. Huang and C. T. Sun, Philos. Mag. **91**, 981 (2011).

[7] X. N. Liu, G. K. Hu, G. L. Huang, and C. T. Sun, Appl. Phys. Lett. **98**, 251907 (2011).

[8] M. I. Hussein, M. J. Leamy, and M. Ruzzene, Appl. Mech. Rev. **66**, 040802 (2014).

[9] M. Dubois, E. Bossy, S. Enoch, S. Guenneau, G. Lerosey, and P. Sebbah, Phys. Rev. Lett. **114**, 013902 (2015).

[10] A. Colombi, P. Roux, S. Guenneau, and M. Rupin, J. Acoust. Soc. Am. **137**, 1783 (2015).

[11] N. Kaina, F. Lemoult, M. Fink, and G. Lerosey, Nature (London) **525**, 77 (2015).

[12] P. Wang, L. Lu, and K. Bertoldi, Phys. Rev. Lett. **115**, 104302 (2015).

[13] S. H. Mousavi, A. B. Khanikaev, and Z. Wang, Nat. Commun. **6**, 8682 (2015).

[14] R. Süsstrunk and S. D. Huber, Science **349**, 47 (2015).

[15] Z. Yang, F. Gao, X. Shi, X. Lin, Z. Gao, Y. Chong, and B. Zhang, Phys. Rev. Lett. **114**, 114301 (2015).

[16] H. He, C. Qiu, L. Ye, X. Cai, X. Fan, M. Ke, F. Zhang, and Z. Liu, Nature (London) **560**, 61 (2018).

[17] M. Tsimokha, V. Igoshin, A. Nikitina, I. Toftul, K. Frizyuk, and M. Petrov, Phys. Rev. B **105**, 165311 (2022).

[18] Z.-Q. Wang, Q.-B. Liu, X.-F. Yang, and H.-H. Fu, Phys. Rev. B **106**, L161302 (2022).

[19] M. Wang, S. Liu, Q. Ma, R.-Y. Zhang, D. Wang, Q. Guo, B. Yang, M. Ke, Z. Liu, and C. T. Chan, Phys. Rev. Lett. **128**, 246601 (2022).

[20] J.-J. Liu, Z.-W. Li, Z.-G. Chen, W. Tang, A. Chen, B. Liang, G. Ma, and J.-C. Cheng, Phys. Rev. Lett. **129**, 084301 (2022).

[21] F. Lucklum and M. Vellekoop, Proc. Eng. **120**, 1095 (2015).

[22] F. Lucklum and M. J. Vellekoop, IEEE Trans. Ultrason. Ferroelectr. Freq. Control **63**, 796 (2016).

[23] F. Lucklum and M. J. Vellekoop, Crystals **7**, 348 (2017).

[24] O. McGee, H. Jiang, F. Qian, Z. Jia, L. Wang, H. Meng, D. Chronopoulos, Y. Chen, and L. Zuo, Addit. Manuf. **30**, 100842 (2019).

[25] M. Askari, D. A. Hutchins, P. J. Thomas, L. Astolfi, R. L. Watson, M. Abdi, M. Ricci, S. Laureti, L. Nie, S. Freear, R. Wildman, C. Tuck, M. Clarke, E. Woods, and A. T. Clare, Addit. Manuf. **36**, 101562 (2020).

[26] I. Arretche and K. H. Matlack, J. Sound Vib. **540**, 117305 (2022).

[27] Z. Liu, X. Zhang, Y. Mao, Y. Y. Zhu, Z. Yang, C. T. Chan, and P. Sheng, Science **289**, 1734 (2000).

[28] Z. Liu, C. T. Chan, and P. Sheng, Phys. Rev. B **71**, 014103 (2005).

[29] Z. Yang, J. Mei, M. Yang, N. H. Chan, and P. Sheng, Phys. Rev. Lett. **101**, 204301 (2008).

[30] G. Ma and P. Sheng, Sci. Adv. **2**, e1501595 (2016).

[31] K. L. S. Yip and S. John, Phys. Rev. B **104**, 054302 (2021).

[32] When the mass of the spring is not negligible, the coupling between the shell and the core is represented by a more general Hermitian matrix. The effective mass, in the leading order correction in the mass of the spring, retains the same algebraic form in Eq. (5a), with first-order shifts in the characteristic frequencies.

[33] Intuitively, the translational oscillation of the rod is coupled to the rotational oscillation of the box, owing to the off-center position of the springs. It can be verified that, in the special case of reflection symmetry $a = 0$, the effective inertia tensor is diagonal. More precisely, the total angular momentum of the resonator, pivoted at the center of mass of the box (center of the left sidewall), contains the term $\mathbf{r}_c \times \mathbf{p}_c$, where $\mathbf{r}_c$ denotes the position of the rod center-of-mass relative to the box center of mass, and $\mathbf{p}_c$ denotes the linear momentum of the rod. Rotational oscillation of the shell invariably excites simultaneously the translational and rotational oscillations of the interior rod.

[34] P. Peng, J. Mei, and Y. Wu, Phys. Rev. B **86**, 134304 (2012).

[35] K. L. S. Yip and S. John, Phys. Rev. B **103**, 094304 (2021).

[36] L. Landau, E. Lifshitz, A. Kosevich, J. Sykes, L. Pitaevskii, and W. Reid, *Theory of Elasticity: Volume 7*, Course of Theoretical Physics (Elsevier Science, Oxford, UK, 1986).

[37] The linear spring constant is determined by an elastostatic equilibrium: $\kappa = [24\pi\mu(\lambda + 2\mu)(\lambda + 4\mu)R_1R_2(R_2^5 - R_1^5)]/\{(R_2 - R_1)^2[\lambda^2(R_2 - R_1)^2(4R_1^2 + 7R_1R_2 + 4R_2^2) + 2\lambda\mu(13R_1^4 + 8R_1R_2^3 + 3R_1^2R_2^2 + 8R_1^3R_2 + 13R_2^4) + 5\mu^2(8R_1^4 + 7R_1^3R_2 + 6R_1^2R_2^2 + 7R_1R_2^3 + 8R_2^4)]\}$.

[38] The relevant lengths are $R_1 = 5$ mm and $R_2 = 7.5$ mm. The Lamé parameters of silicone are $\lambda = 6 \times 10^5$ Pa, $\mu = 4 \times 10^4$ Pa. The density of lead is $\rho_c = 11\,600$ kg m^{-3}. These material constants are taken from footnote 8 in Ref. [27].

[39] When the core rotates from equilibrium $\Phi_s\hat{\mathbf{z}}$ and the shell by $\Phi_s\hat{\mathbf{z}}$, the displacement field in spherical coordinates $\mathbf{u}(\mathbf{r}) = u_\phi(r)\sin\theta\hat{\boldsymbol{\phi}}$, with $R_1 < r < R_2$, satisfies elastostatic equilibrium under the boundary conditions $\mathbf{u}(R_{1/2}) = R_{1/2}\Phi_{c/s}\sin\theta\hat{\boldsymbol{\phi}}$. The second-order linear boundary-value problem governing $u_\phi(r)$ is solved in terms of elementary functions. The torque acting on the core/shell is determined by a surface integral of the moments generated by the stress field on $\{r = R_{1/2}\}$.

[40] A. Chutinan and S. John, Phys. Rev. A **78**, 023825 (2008).

[41] S. Eyderman, A. Deinega, and S. John, J. Mater. Chem. A **2**, 761 (2014).

[42] S. Foster and S. John, J. Appl. Phys. **120**, 103103 (2016).

[43] The remaining nonvanishing effective inertia components of the dumbbell resonator are $m_{44}(f) = I_{x,\mathrm{db}} + \frac{I_{c1}f_{0,\mathrm{r}1}^2}{f_{0,\mathrm{r}1}^2 - f^2} + \frac{I_{c2}f_{0,\mathrm{r}2}^2}{f_{0,\mathrm{r}2}^2 - f^2} + \frac{a^2}{4}\left(\frac{m_{c1}f_{0,\mathrm{t}1}^2}{f_{0,\mathrm{t}1}^2 - f^2} + \frac{m_{c2}f_{0,\mathrm{t}2}^2}{f_{0,\mathrm{t}2}^2 - f^2}\right)$, $m_{66}(f) = I_{z,\mathrm{db}} + \frac{I_{c1}f_{0,\mathrm{r}1}^2}{f_{0,\mathrm{r}1}^2 - f^2} + \frac{I_{c2}f_{0,\mathrm{r}2}^2}{f_{0,\mathrm{r}2}^2 - f^2}$, and $m_{15}(f) = \frac{a}{2}\left(\frac{m_{c1}f_{0,\mathrm{t}1}^2}{f_{0,\mathrm{t}1}^2 - f^2} - \frac{m_{c2}f_{0,\mathrm{t}2}^2}{f_{0,\mathrm{t}2}^2 - f^2}\right)$, where $m_{33}(f) = m_{11}(f) = m_{22}(f)$, $m_{44}(f) = m_{55}(f)$, $m_{15}(f) = m_{51}(f) = -m_{24}(f) = -m_{42}(f)$, $I_{c1} = (2/5)m_{c1}R_1^2$, $I_{c2} = 1.02I_{c1}$, $I_{s,x} \approx 21.00$ mg mm^2, and $I_{s,z} \approx 7.512$ mg mm^2.